PHYSICAL REVIEW B **93**, 045117 (2016)

Biased doped silicene as a way to tune electronic conduction

Y. G. Pogorelov[1] and V. M. Loktev[2,3]
[1] *IFIMUP-IN, Departamento de Física, Universidade do Porto, Portugal*
[2] *Bogolyubov Institute for Theoretical Physics, National Academy of Sciences of Ukraine, Kyiv, Ukraine*
[3] *National Technical University of Ukraine "Kyiv Polytechnic Institute", Kyiv, Ukraine*

(Received 17 September 2015; revised manuscript received 22 November 2015; published 15 January 2016)

Restructuring of the electronic spectrum in a buckled silicene monolayer under some applied voltage between its two sublattices and in the presence of certain impurity atoms is considered. Special attention is given to formation of localized impurity levels within the band gap and to their collectivization at finite impurity concentration. It is shown that a qualitative restructuring of the quasiparticle spectrum within the initial band gap and then specific metal-insulator phase transitions are possible for such disordered system and can be effectively controlled by variation of the electric field bias at a given impurity perturbation potential and concentration. Since these effects are expected at low impurity concentrations but at not too low temperatures, they can be promising for practical applications in nanoelectronic devices.

DOI: 10.1103/PhysRevB.93.045117

I. INTRODUCTION

After the revolutionary breakthrough of graphene, introducing unusual relativistic effects into solid state physics [1], the family of relative materials is continuously growing. In particular, a possibility of obtaining new semiconducting materials where the band gap can be tuned by external electric bias is extensively studied. This was first demonstrated for the graphene bilayer, called bigraphene [2]. Unlike the basic monolayer graphene, here a nonequivalence of two sublayers takes place under electric field applied normally to them. Opening of a tunable semiconducting gap and perspectives of its practical use in tunable transistors is now broadly discussed. The same possibility was already indicated in a variety of similar systems, including even single layered, as, for instance, silicene, the Si-based analog of graphene [3]. Its important structural difference from graphene consists in a much more pronounced buckling of its 2D hexagonal lattice, thus leading to a nonequivalence of two sublattices in the same layer and to opening of a band gap under normal-to-plane electric bias [4–6,10]. Subsequently, fabrication of practical field-effect transistors based on a silicene sheet is extensively sought [7–10].

When comparing these 2D systems with common semiconductors, an important question arises on their behavior under doping by impurity atoms. As is well known, such doping in common semiconductors produces localized in-gap energy levels near the edges of the conduction band (called donor levels) or valence band (acceptor levels) [11]. For the mostly used dopants (such as Si neighbors from the periodic table) these levels are very shallow (of some tens of meV depth compared to some eV bandwidths) so that charge carriers can be thermally excited from them to the nearby band (conduction or valence) and thus contribute into conduction of respective kinds (electron or hole). The resulting conductivity turns sensitive to external bias realized in specific devices, defining their effectiveness [12]. The typical dopant concentration n is quite low and, in order to assure the mean distance $\bar{r} = n^{-1/3}$ between dopants to surpass the long effective radius of localized state $r_{\mathrm{loc}} \gg a$ (the lattice parameter), it should not exceed $n_0 = r_{\mathrm{loc}}^{-3} \sim 10^{17}\,\mathrm{cm}^{-3}$ (for 3D systems). Then it is known that for $n \gg n_0$ the doped system is brought to metallization [13], due to growing interaction between dopants and subsequent broadening of the dopant level. Hence the Fermi level, initially fixed at the dopant level, becomes displaced to the band interior. This phenomenon is generally considered adverse for electronics purposes, since it drastically reduces the bias sensitivity. Otherwise, alternative types of impurities (such as transition and rare-earth elements), producing the so called deep levels in the semiconducting gap [14], are not effective for thermalization of carriers and instead can act as traps for them.

The above limitations however can be effectively overcome under the possibility of tuning the fundamental band gap and also other relevant spectrum characteristics such as the Fermi level and the Mott mobility edges [15]. This opens a formerly unexplored perspective of bringing the bias sensitivity of conduction to a much broader scale than in common semiconductors, spanning from metallic to insulating regimes through the Mott metal-insulator transition (MIT). The purpose of the present study is to illustrate such an expectation on the particular example of biased and doped silicene, considering both situations of shallow and deep dopant levels with their specific regimes. Though a detailed treatment of these issues, using the realistic impurity potentials, their screening by relativistic electrons, etc., can present certain technical problems, it can be much facilitated with the use of simplified models, traditionally applied for impurities both in common semiconductors and in graphene-related materials. Such are the Lifshitz model [16], better suited for shallow dopants, and the Anderson hybrid model [17], more adequate for deep dopants. Below we analyze the electronic spectra of biased and doped silicene within these two models and indicate possible tuning regimes to reach desirable effects.

II. FORMULATION OF THE PROBLEM

For the silicene hexagonal lattice with two nonequivalent sites in a unit cell (Fig. 1), we write down the tight-binding Hamiltonian as

$$H_0 = \sum_{\mathbf{k}} \psi_{\mathbf{k}}^{\dagger} \hat{h}_{\mathbf{k}} \psi_{\mathbf{k}}. \tag{1}$$

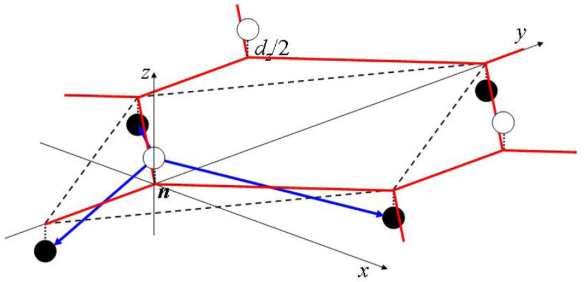

FIG. 1. Crystalline structure of a buckled silicene plane where silicon atoms are up- or down-shifted by $d_z/2$ from the initial hexagonal plane (red lines). The dashed line delimits a unit cell at the position $\mathbf{n}$ with two nonequivalent sites, of A type (clear) and B type (dark); blue arrows indicate three vectors $\boldsymbol{\delta}$ between nearest-neighbor Si atoms.

Here 2-spinors $\psi_{\mathbf{k}}^{\dagger} = (a_{\mathbf{k}}^{\dagger}, b_{\mathbf{k}}^{\dagger})$ are made of 2D Fourier transforms $a_{\mathbf{k}} = N^{-1/2}\sum_{\mathbf{n}} e^{i\mathbf{k}\cdot\mathbf{n}} a_{\mathbf{n}}$ and $b_{\mathbf{k}} = N^{-1/2}\sum_{\mathbf{n}} e^{i\mathbf{k}\cdot\mathbf{n}} b_{\mathbf{n}}$ of local Fermi operators at A- and B-type sites in the **n**th unit cell (N is the total number of cells). The 2×2 Pauli matrix expansion $\hat{h}_{\mathbf{k}} = \hat{\sigma}_{+} t_{\mathbf{k}} + \hat{\sigma}_{-} t_{\mathbf{k}}^{*} + \hat{\sigma}_{3} V/2$ includes the complex factors $t_{\mathbf{k}} = t\sum_{\boldsymbol{\delta}} e^{i\mathbf{k}\cdot\boldsymbol{\delta}}$, due to the hopping amplitude $t \sim 1.1$ eV between nearest-neighbor sites separated by the vectors $(\boldsymbol{\delta}, d_z)$ with their xy-plane components $|\boldsymbol{\delta}| = a \approx 0.22$ nm and normal buckling components $d_z \sim 0.2a$ [18,19]. Also here are the on-site energy shifts $\pm V/2$, due to the effect of buckling and external electric field, referred to as bias in what follows, this field supposed to result from combined top and back gates and not to influence the charge density. For the sake of simplicity, relatively weak spin-orbit interactions (able to produce an intrinsic band gap of a few meV [20]) and so spin degrees of freedom are omitted in Eq. (1) but their possible effects are discussed in the last section below.

The relevant low-energy physics is generated near the nodal points $\pm\mathbf{K} = (\pm 4\pi/3\sqrt{3}a, 0)$ in the Brillouin zone so that for $\mathbf{q} = \mathbf{k} - \mathbf{K}$ with $aq \ll 1$ we have $t_{\mathbf{k}} \approx \hbar v_{\mathrm{F}} q e^{-i\varphi_{\mathbf{q}}}$ where the Fermi velocity $v_{\mathrm{F}} = 3at/(2\hbar)$ and $\varphi_{\mathbf{q}} = \arctan q_y/q_x$.

We study electronic states in this system using the Green's function (GF) matrix $\hat{G}(\mathbf{k},\mathbf{k}') = \langle\langle \psi_{\mathbf{k}} | \psi_{\mathbf{k}'}^{\dagger} \rangle\rangle$ that satisfies the equation of motion,

$$\varepsilon \hat{G}(\mathbf{k},\mathbf{k}') = \langle\{\psi_{\mathbf{k}}, \psi_{\mathbf{k}'}^{\dagger}\}\rangle + \langle\langle [\psi_{\mathbf{k}}, H] | \psi_{\mathbf{k}'}^{\dagger} \rangle\rangle, \tag{2}$$

for the full Hamiltonian H. Generally, the GF matrix defines the system energy spectrum by the roots of the general dispersion equation: $\mathrm{Re}\det\hat{G} = 0$, that is, by the poles of its diagonal elements in the basis of exact eigen-states, and the total density of states (DOS) is defined as

$$\rho(\varepsilon) = \frac{1}{2\pi N}\mathrm{Tr}\,\mathrm{Im}\,\hat{G}, \tag{3}$$

in any basis. Using Eq. (2) with the unperturbed Hamiltonian, $H = H_0$, Eq. (1), leads to a momentum-diagonal form for the nonperturbed GF matrix $\hat{G}^{(0)}(\mathbf{k},\mathbf{k}') = \delta_{\mathbf{k},\mathbf{k}'}\hat{G}_{\mathbf{k}}^{(0)}$, where

$$\hat{G}_{\mathbf{k}}^{(0)} = \frac{\varepsilon + \hat{h}_{\mathbf{k}}}{\varepsilon^2 - V^2/4 - \xi^2}, \tag{4}$$

and $\xi_{\mathbf{k}} = |t_{\mathbf{k}}|$ is an effective momentum variable for the relevant low-energy range, $|\varepsilon| \ll \Lambda$ (where $\Lambda = \hbar v_{\mathrm{F}}\sqrt{K/a} = t\sqrt{\pi\sqrt{3}}$ is the bandwidth, that is, an energy cutoff). In this approximation, the electronic spectrum consists of two symmetric bands $\pm\varepsilon_0(\xi) = \pm\sqrt{V^2/4 + \xi^2}$ with a gap of V between them. The related nonperturbed DOS is linear beyond this gap,

$$\rho_0(\varepsilon) = \frac{\varepsilon}{\Lambda^2}\theta(V^2/4 - \varepsilon^2)\theta(\Lambda^2 + V^2/4 - \varepsilon^2), \tag{5}$$

and normalized: $\int_{-\infty}^{\infty}\rho_0(\varepsilon)d\varepsilon = 1$. This situation in silicene with a buckled lattice is referred to as realization of a tunable gap between the lower (valence) band and the higher (conduction) band, in contrast to a fixed gap in common semiconductors (such as crystalline Si).

Now we pass to the specifics of doping this system by impurity atoms at random sites within its crystalline lattice that produce its perturbation through the above mentioned Lifshitz and Anderson models.

III. LIFSHITZ MODEL

We begin with the simpler Lifshitz model [16] characterized by a single perturbation parameter, the on-site energy shift U on all impurity atoms located at $\mathbf{p}_1$ sites in the first sublattice and $\mathbf{p}_2$ sites in the second sublattice with relative concentrations $c_{1,2}$ (both expectedly small, $c_j \ll 1$). Such substitutional type better corresponds to impurities such as Si neighbors in the periodic table. The corresponding Lifshitz perturbation reads

$$H_L = \frac{1}{N}\sum_{\mathbf{k},\mathbf{k}'}\sum_{j,\mathbf{p}_j} e^{i(\mathbf{k}'-\mathbf{k})\cdot\mathbf{p}_j}\psi_{\mathbf{k}}^{\dagger}\hat{U}_j\psi_{\mathbf{k}'}, \tag{6}$$

with the scattering matrices $\hat{U}_j = U\hat{p}_j$ and the sublattice projectors $\hat{p}_{1,2} = (1 \pm \hat{\sigma}_z)/2$. In this model with the full Hamiltonian $H = H_0 + H_L$, the explicit equation of motion for the momentum-diagonal GF matrix,

$$\hat{G}(\mathbf{k}) = \hat{G}^{(0)}(\mathbf{k}) + \frac{1}{N}\sum_{j,\mathbf{p}_j,\mathbf{k}'} e^{i(\mathbf{k}'-\mathbf{k})\cdot\mathbf{p}_j}\hat{G}_{\mathbf{k}}^{(0)}\hat{U}_j\hat{G}(\mathbf{k}',\mathbf{k}), \tag{7}$$

leads to the standard solution:

$$\hat{G}_{\mathbf{k}} = \left[\left(\hat{G}_{\mathbf{k}}^{(0)}\right)^{-1} - \Sigma_{1,\mathbf{k}}\hat{p}_1 - \Sigma_{2,\mathbf{k}}\hat{p}_2\right]^{-1}. \tag{8}$$

Here the partial self-energy functions are presented by their respective group expansions (GEs) [21]:

$$\Sigma_{j,\mathbf{k}} = c_j T_j (1 + c_j B_{j,\mathbf{k}} + \cdots), \tag{9}$$

where the partial T matrix $T_j = U/(1 - Ug_j)$ with local GFs $g_j = N^{-1}\sum_{\mathbf{k}}(\hat{G}_{\mathbf{k}})_{jj}$ describes the effects of multiple scatterings on a single impurity center. It can be generally shown that the GE series, Eq. (9), is converging within the energy range of bandlike states and can be well approximated there by its first T-matrix term while the rest of terms are important for the check of convergence. The first of the nontrivial GE terms is due to impurity pairs,

$$B_{j,\mathbf{k}} = \sum_{\mathbf{n}\neq 0}\frac{A_{j,\mathbf{n}}e^{-i\mathbf{k}\cdot\mathbf{n}} + A_{j,\mathbf{n}}A_{j,-\mathbf{n}}}{1 - A_{j,\mathbf{n}}A_{j,-\mathbf{n}}}, \tag{10}$$

and includes the functions of interimpurity interaction: $A_{j,\mathbf{n}} = T_j N^{-1}\sum_{\mathbf{k}'\neq\mathbf{k}} e^{i\mathbf{k}'\cdot\mathbf{n}}(\hat{G}_{\mathbf{k}'})_{jj}$. It should be also noted that all the products of these functions in the expansion of Eq. (10) are presented by multiple sums in *noncoinciding* momenta [21,22]. The omitted terms in the parentheses of Eq. (9) correspond to clusters of three and more impurities; they are expressed through respective combinations of these functions.

Generally, once the initial translation symmetry of the crystalline lattice is broken by the presence of impurities, the quasimomentum is no longer an exact quantum number and also the system spectrum is not limited to the initial bands, since already a single impurity can produce localized levels beyond the bands. However, for not too strong a disorder, this spectrum maintains continuous ranges of bandlike states (both the modified initial bands and possibly some new impurity bands arising near localized levels), intercalated by the ranges of truly localized states (either on single impurities or on their clusters). Within bandlike ranges, the approximate dispersion laws of corresponding subbands $\varepsilon_j(\xi)$ (in our case, $j = 1,2$, *imp* for two initial and impurity bands, respectively) are given by the formal roots of the above mentioned dispersion equation in the $\mathbf{k}$ basis:

$$\mathrm{Re}\det \hat{G}_{\mathbf{k}} = 0. \tag{11}$$

However their validity is restricted by the known Ioffe-Regel-Mott (IRM) criterion [15,23] that for this case takes the form

$$\xi d\varepsilon_j(\xi)/d\xi \gg \Gamma_j(\xi) \tag{12}$$

with the damping term $\Gamma_j(\xi) = \mathrm{Im}\Sigma_{j,\mathbf{k}}$ for $\xi = \xi_{\mathbf{k}}$. The separation points between the extended and localized ranges, called Mott mobility edges, are estimated from the condition that the symbol "$\gg$" in Eq. (12) is changed for "$\sim$", ending validity of the IRM criterion. This also qualitatively agrees with a similar change in the convergence criterion for GE: $c|B_{j,\mathbf{k}}| \ll 1$. Within the band gap, the broadening Γ_j mainly results from $\mathrm{Im}\, B_{j,\mathbf{k}}$ in Eq. (9), so analysis of this range needs calculation of the functions g_j and $A_{j,\mathbf{n}}$. A reasonable approximation for them follows from substitution of $\hat{G}_{\mathbf{k}}$ by $\hat{G}^{(0)}_{\mathbf{k}}$ in corresponding sums resulting in

$$g_{1,2} \approx \frac{\varepsilon \pm V/2}{\Lambda^2} \ln \frac{V^2/4 - \varepsilon^2}{\Lambda^2} \tag{13}$$

and

$$A_{j,\mathbf{n}} \approx \frac{(\varepsilon \pm V/2)T_j}{\Lambda^2} K_0(|\mathbf{n}|/r_\varepsilon) \tag{14}$$

(see details in the Appendix). Here the characteristic length $r_\varepsilon = \hbar v_{\mathrm{F}}/\sqrt{V^2/4 - \varepsilon^2}$ and the McDonald function $K_0(x)$ has asymptotics [24]:

$$K_0(x) \approx \begin{cases} \ln(2/x) - \gamma, & x \ll 1, \\ \sqrt{2/(\pi x)}e^{-x}, & x \gg 1, \end{cases}$$

with the Euler's constant $\gamma \approx 0.5772$.

The logarithmic divergence of g_j, Eq. (13), near one of the gap edges allows a localized level $\varepsilon_{\mathrm{loc}}$ to appear there under a proper impurity perturbation. Thus, if one chooses for definiteness $U < 0$ (and supposedly $|U| \lesssim \Lambda$), this level is due to the pole of T_1 (by impurities in the first sublattice) near the upper edge $V/2$, their separation being well approximated as

$$V/2 - \varepsilon_{\mathrm{loc}} \approx \frac{\Lambda^2}{V} e^{-\Lambda^2/(|U|V)} \equiv c_0 \frac{\Lambda^2}{V}. \tag{15}$$

Hence the localized level is exponentially shallow for all practically achievable bias values (always $V \ll \Lambda$), which can justify such modeling of real shallow levels. At this choice, another term T_2 (by impurities in the second sublattice) has no poles and is less relevant.

Further analytical study of the modified spectrum uses some approximated energy dependencies of the relevant T_1 matrix. Thus, in a close enough vicinity to the localized level, $|\varepsilon - \varepsilon_{\mathrm{loc}}| \ll V/2 - \varepsilon_{\mathrm{loc}}$, its denominator can be linearized,

$$T_1 \approx \frac{\Lambda^2(V/2 - \varepsilon_{\mathrm{loc}})}{V(\varepsilon - \varepsilon_{\mathrm{loc}})}, \tag{16}$$

while in a wider area, $0 < V/2 - \varepsilon \ll V$, the logarithmic approximation applies:

$$T_1 \approx \frac{\Lambda^2}{V} \ln^{-1} \frac{V/2 - \varepsilon_{\mathrm{loc}}}{V/2 - \varepsilon}. \tag{17}$$

At last, when considering the energy scales over the whole band gap, $|\varepsilon| \gtrsim V$, the complete formula, Eq. (13), should be used in the T matrices.

Of course, for $U > 0$, symmetric formulas with respect to Eqs. (15)–(17) apply for the pole of T_2 near the lower gap edge and for its related vicinities while T_1 becomes irrelevant.

Let us focus now on the most restructured region of spectrum, including the impurity band $\varepsilon_{\mathrm{imp}}(\xi)$ and its closest neighbor areas of $\varepsilon_{1,2}(\xi)$ bands. In this course, it is convenient to consider this restructuring with growing bias V at fixed impurity parameters U and c. The T-matrix approximation $\Sigma_{j,\mathbf{k}} \approx c_j T_j$ is sufficient at the first step, as far as the quasiparticle lifetime and respective IRM limits for bandlike states are not considered.

At lowest bias $V \ll c|U|$, the numerical solution of the dispersion equation, Eq. (11), with use of Eq. (13), shows the spectrum restructuring to be very close to its simple shift by cU; that is, the impurity effect is reduced to that of the effective medium potential. Formally, this solution includes the impurity band $\varepsilon_{\mathrm{imp}}(\xi)$ of $c|U|$ width and separately the modified upper subband $\varepsilon_1(\xi)$. However, it is seen from Fig. 2 [inset (a)] that their composition is closely matched near the $\varepsilon_{\mathrm{loc}}$ level and practically coincides with a single shifted law: $\varepsilon_{\mathrm{comp}}(\xi) = \sqrt{V^2/4 + \xi^2} + cU$, attaining its lower edge at $\xi = 0$: $\varepsilon_g \equiv \varepsilon_{\mathrm{comp}}(0) = V/2 + cU$. As seen from Fig. 2 [inset (b)], such composite $\varepsilon_1 + \varepsilon_{\mathrm{imp}}$-band structure persists for low enough bias such that $c \ll c_0$, and, using Eq. (15), this relates to $V \ll V_A = \Lambda^2/(|U \ln c|)$ (the latter value to be explained below). Noting from Eq. (14) at $\varepsilon = \varepsilon_{\mathrm{loc}}$ that the localization radius is $r_{\mathrm{loc}} = \hbar v_{\mathrm{F}}/(\Lambda\sqrt{c_0})$, this refers to $r_{\mathrm{loc}} \ll \bar{r} = \hbar v_{\mathrm{F}}/(\Lambda\sqrt{\pi c})$, a 2D analogy to the metallization condition discussed in the Introduction. Thus, the characteristic concentration c_0 (in fact, an analog to n_0 in the Introduction) is bias tuned, and a tuned Anderson transition on the $\varepsilon_{\mathrm{imp}}$ band (merger of its mobility edges and vanishing of bandlike states [17]) is expected at the bias value V_A.

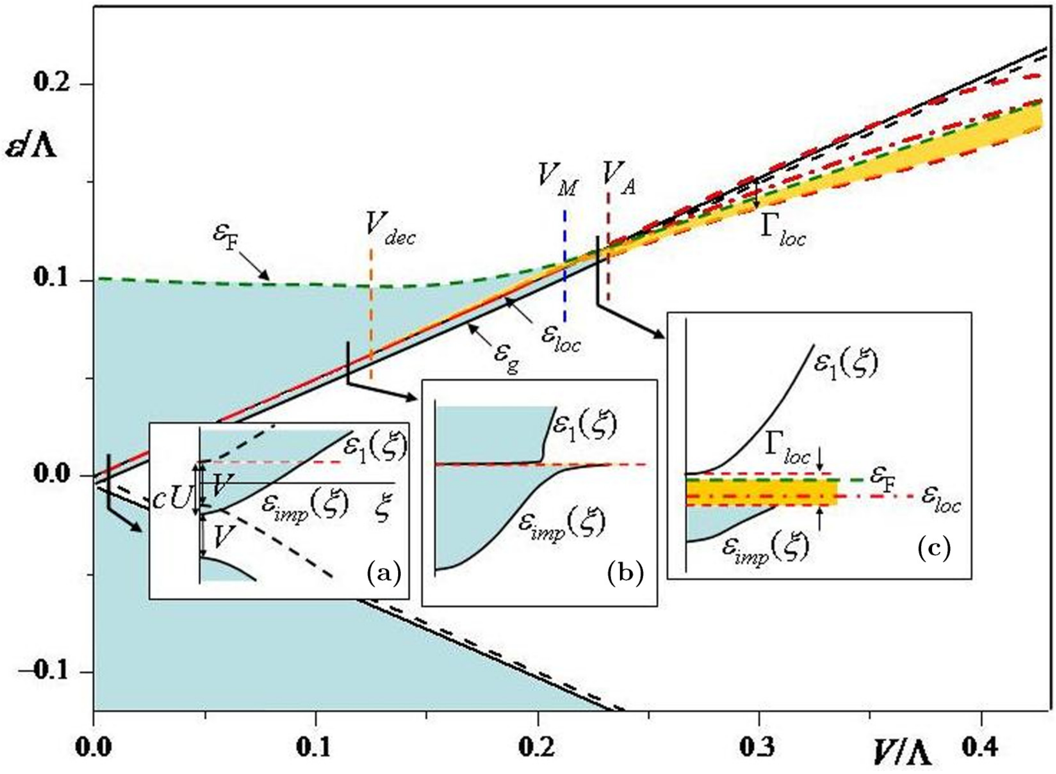

FIG. 2. Spectrum restructuring in silicene with Lifshitz impurities at the choice of their parameters $U = -\Lambda$ and $c = 0.01$ as a function of the bias V. Insets show the particular dispersion laws as a function of the momentum variable ξ at (a) weak ($V = 0.004\Lambda$), (b) medium ($V = 0.11\Lambda$), and (c) strong ($V = 0.23\Lambda$) bias. Black lines mark the edges of conduction and valence bands (dashed in absence and solid in presence of impurities). Blue areas present filled bandlike states and golden filled localized states, limited from above by the Fermi level (green dashed line); red dashed lines mark the concentration broadening of impurity level. Vertical dashed lines indicate the critical bias levels: $V_{\rm dec}$ for the band decomposition (orange), V_M for the Mott (blue), and V_A for the Anderson (purple) phase transitions.

At growing bias up to $V \gg c|U|$, the composite band structure can be described with use of Eq. (17). Then the renormalized dispersion law $\varepsilon = \varepsilon_{\rm imp}(\xi)$ follows from Eq. (11) in an implicit form as

$$\frac{V^2}{4} - \varepsilon_{\rm imp}^2(\xi) = \left(\frac{V^2}{4} - \varepsilon_{\rm loc}^2\right)\exp\left(\frac{c\Lambda^2}{\frac{V^2}{4} - \varepsilon_{\rm imp}^2(\xi) + \xi^2}\right). \tag{18}$$

This equation permits analytic solutions near the edges of the $\varepsilon_{\rm imp}$ band. Thus, the lower edge corresponds to $\xi \to 0$:

$$\varepsilon_g \equiv \varepsilon_{\rm imp}(0) \approx \frac{V}{2} - \frac{c\Lambda^2}{V\,W(c/c_0)}, \tag{19}$$

where $W(z)$ is the Lambert W function [25]. Its asymptotics, $W(z \gg 1) \approx \ln(z/\ln z)$, used in Eq. (19) provide a simpler function:

$$\varepsilon_g \approx \frac{V}{2} + cU\left[1 - \frac{\ln c}{\ln(cc_0)}\frac{V}{V_A}\right], \tag{20}$$

replacing the above linear ε_g dependence at $V \ll c|U|$ in the wider range of $V \ll V_A$. At yet higher bias, up to $V \sim V_A$, the full Eq. (19) applies.

Expanding Eq. (18) at $\xi^2 \ll V^2/4 - \varepsilon_g^2$, the long-wave dispersion law is obtained:

$$\varepsilon_{\rm imp}(\xi) \approx \varepsilon_g + \left(1 + \frac{V^2}{4c\Lambda^2}\right)^{-1}\frac{\xi^2}{2\varepsilon_g}, \tag{21}$$

indicating the $\varepsilon_{\rm comp}$ behavior for $V \ll \sqrt{c}\Lambda$. The further growth of $\varepsilon_{\rm imp}(\xi)$ finally reaches the short-wave asymptotics (at $\xi^2 \gg c\Lambda^2$):

$$\varepsilon_{\rm imp}(\xi) \approx \varepsilon_{\rm loc} - c\Lambda^2\frac{V/2 - \varepsilon_{\rm loc}}{\xi^2}. \tag{22}$$

This defines its formal upper edge $\varepsilon_f = \varepsilon_{\rm imp}(\Lambda) \approx \varepsilon_{\rm loc} - c(V/2 - \varepsilon_{\rm loc})$[26], and then the total width of the impurity band:

$$\Lambda_{\rm imp} \approx \varepsilon_f - \varepsilon_g \approx \frac{\Lambda^2}{V}\left(\frac{c}{W(c/c_0)} - c_0\right). \tag{23}$$

Growing with V from the initial value of $c|U|$, $\Lambda_{\rm imp}$ by Eq. (23) would reach a maximum at some bias value $V_* = F(c)\Lambda^2/|U|$ with the factor $F(c)$ varying from ≈0.12 to ≈0.22 in the range of $10^{-4} < c < 0.1$. However, such V_* is already close to the critical value V_A and hence to the impurity band collapse, making this maximum meaningless.

The next step is to determine the lifetimes of the obtained quasiparticle states, in order to establish the IRM limits for their existence. For the quasiparticle with energy $\varepsilon = \varepsilon_{\text{comp}}(\xi)$, we can consider its effective broadening:

$$\Gamma_{\text{comp}}(\varepsilon) = \operatorname{Im} \frac{cU}{1 - Ug_1(\varepsilon - cU)} \approx \frac{\pi c}{2}\left(\frac{U}{\Lambda}\right)^2 \frac{(V/2 + \varepsilon - cU)^2}{\varepsilon - cU}. \tag{24}$$

Using it in the IRM criterion, Eq. (12), we estimate the location of the mobility edge ε_c near the bottom of ε_{imp}: $\varepsilon_c - \varepsilon_g \sim cU^2V/\Lambda^2$. This distance is negligible beside the width V of the gap between the ε_2 and ε_{imp} bands and the width Λ_{imp} of the ε_{imp} band. However, the broadening, Eq. (24), at $\varepsilon \approx \varepsilon_{\text{loc}}$ much exceeds the formal gap $\approx V/2 - \varepsilon_{\text{loc}}$ (here exponentially small) between the ε_{imp} and ε_1 bands. This permits us to consider such a gap and the very level ε_{loc} nonexisting and justifies the concept of a composite band in the weak bias regime [see insets (a) and (b) in Fig. 2].

The overall electronic state of the doped system is determined by the location of its Fermi level ε_{F} with respect to the mobility edges. Supposing each impurity atom to supply one carrier to the system and $\varepsilon_{\text{F}} = 0$ in the undoped state, its position at finite c is found from the equation

$$c = 2\int_{\varepsilon_g}^{\varepsilon_{\text{F}}} \rho(\varepsilon)d\varepsilon \tag{25}$$

(including the spin factor 2). For the weak bias regime (or, in other words, for $c_0 \ll c$), one can use here the composite band DOS, $\rho(\varepsilon) \approx \rho_0(\varepsilon + \varepsilon_g)$, and obtain the bias-dependent Fermi level within this band as

$$\varepsilon_{\text{F}}(V) \approx \sqrt{c\Lambda^2 + \varepsilon_g^2}. \tag{26}$$

At low enough bias, $V \ll \sqrt{c}\Lambda$, it lies as high within the $\varepsilon_{\text{comp}}$ band as $\varepsilon_{\text{F}} \approx \sqrt{c}\Lambda$ (Fig. 2) and defines a metallic behavior of the system. This can be just compared to metallization of common semiconductors at high enough doping ($c \gg c_0$).

With growing bias, $\varepsilon_{\text{F}}(V)$ gets closer to the band's bottom ε_g but its expected crossing of a mobility edge and the system transition into insulating state can be only reached after the decomposition of ε_{imp} and ε_1 bands by means of an emerging localized range around the impurity level ε_{loc}. From comparison of Eqs. (15) and (24), this is estimated to take place at $c \sim c_0 \ln^2(1/c_0)$. The related bias value is high enough:

$$V_{\text{dec}} \sim \frac{\Lambda^2}{2|UW_{-1}(-\sqrt{c}/2)|}, \tag{27}$$

including the lower branch W_{-1} of the multivalued Lambert function with asymptotics $W_{-1}(z) \approx \ln(z/\ln|z|)$ for $-1/e < z < 0$ [25]. However, this V_{dec} is yet well below the ε_{imp}-band collapse value V_A [see inset (c) in Fig. 2]. Then, taking into account the T-matrix contribution to DOS for the lower decomposed subband,

$$\rho_l(\varepsilon) \approx \frac{\varepsilon}{\Lambda^2} - \frac{cc_0\Lambda^2}{2V^2(\varepsilon - \varepsilon_{\text{loc}})}, \tag{28}$$

and using it in Eq. (25), we find the condition that ε_{F} reaches the top of ε_{imp}:

$$c = 2\int_{\varepsilon_g}^{\varepsilon_f} \rho_l(\varepsilon)d\varepsilon \approx \frac{c}{W(c/c_0)} - c_0 + \frac{cc_0\Lambda^2}{2V^2}\ln\left(\frac{1}{c_0W(c/c_0)} - \frac{1}{c}\right). \tag{29}$$

Implicitly, Eq. (29) defines the bias value V_M that can be associated with the tuned MIT, provided this value is above V_{dec} so that the top of ε_{imp} already pertains to the localized range. The MIT bias value is estimated from Eq. (29) as

$$V_M \approx \frac{7\Lambda^2}{4|U|\ln(z_M/c)}, \tag{30}$$

where the factor in the logarithm depends on the perturbation parameter as $z_M \approx (3.35U/\Lambda)^4$, by a reasonable empirical fit. Then, the numerical comparison between Eqs. (27) and (30) shows that V_{dec} in fact precedes V_M for all realistic $U \lesssim \Lambda$. But the sequence of tuned MIT and Anderson transitions can be changed depending on the impurity parameters. So, the $V_M \to V_A$ sequence for their above choice (as in Fig. 2) would pass to $V_A \to V_M$ for $c = 0.01$ and $|U| < 0.71\Lambda$. Such a change turns possible in the given model due to the fact that here the Mott transition results from the Fermi level motion down to the bottom of the main band while the Anderson transition is restricted to the impurity band. With the bias V exceeding V_A, the impurity band does not make sense already but there stays a well defined localized level, Eq. (15), whose width estimated from the GE pair term becomes exponentially small at $c \ll c_0$: $\Gamma_{\text{loc}} \sim c_0(\Lambda^2/V)e^{-c_0/c}$ (see details in the Appendix).

The above discussed tuned restructuring of the spectrum can be summarized as follows. At low bias, $V \ll V_M$, the system is metallized by the impurity doping, with the Fermi level lying deep within the composite $\varepsilon_1 + \varepsilon_{\text{imp}}$ conduction band. At bias reaching V_{dec}, the composite band gets split into the ε_1 and ε_{imp} bands, separated by a range of localized states around the impurity level ε_{loc}. At further growing bias to V_M, the Fermi level crosses the mobility edge above ε_{loc} to produce MIT. After the Anderson transition occurs at $V = V_A$, a single ε_1 conduction (unoccupied) band is left in the spectrum, the Fermi level staying fixed near ε_{loc}. All the critical bias values, V_{dec}, V_M, and V_A, can be reduced by choosing lower impurity concentration, though this reduction is as slow as $\sim 1/\ln(1/c)$ and simultaneously the thermal stability level for MIT is reduced as $k_{\text{B}}T_{\max} \sim c\ln(1/c)\Lambda^2/|U|$.

Now let us consider the alternative scenario, or the Anderson hybrid model.

IV. ANDERSON HYBRID MODEL

In the Anderson model, there are two perturbation parameters: the on-site energy ε_0 for an electron at an impurity atom and its modified hopping amplitude ηt (supposedly $\eta \lesssim 1$) to the nearest-neighbor host sites. Such type of impurity perturbation better corresponds to transition-metal or rare-earth atoms, known to produce deep levels in common Si (for instance, of 0.21 eV below the conduction band bottom for Ti and of 0.39 eV above the valence band top for Pd impurities) [27]. In silicene, these atoms predominantly

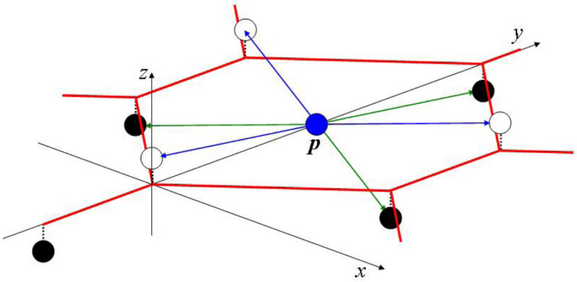

FIG. 3. Anderson impurity at an interstitial position in silicene lattice.

occupy interstitial positions, linked to both host sublattices (see Fig. 3). In the corresponding perturbation Hamiltonian,

$$H_A = \sum_{\mathbf{p}} \left[\varepsilon_0 \alpha_{\mathbf{p}}^\dagger \alpha_{\mathbf{p}} + \frac{1}{\sqrt{N}} \sum_{\mathbf{k}} (e^{i\mathbf{k}\cdot\mathbf{p}} \alpha_{\mathbf{p}}^\dagger \hat{\tau}_{\mathbf{k}}^\dagger \psi_{\mathbf{k}} + \text{H.c.}) \right], \tag{31}$$

this linkage is presented through the 2-spinor $\hat{\tau}_{\mathbf{k}}^\dagger = \eta(t_{\mathbf{k}}, t_{\mathbf{k}}^*)$. The other difference of this model consists of the presence of independent Fermi operators $\alpha_{\mathbf{p}}$ for an electron on impurity site $\mathbf{p}$, besides the above considered host operators in the $\psi_{\mathbf{k}}$ spinor. Subsequently, it generates more involved GF structures (with respect to the sublattice indices): besides the "host" $\hat{G}(\mathbf{k},\mathbf{k}')$ matrices by Eq. (2), here also "impurity" $g_{\mathbf{p},\mathbf{p}'} = \langle\langle \alpha_{\mathbf{p}} | \alpha_{\mathbf{p}'}^\dagger \rangle\rangle$ scalars and "mixed" $h_{\mathbf{k},\mathbf{p}} = \langle\langle \psi_{\mathbf{k}} | \alpha_{\mathbf{p}}^\dagger \rangle\rangle$ and $h_{\mathbf{p},\mathbf{k}}^\dagger = \langle\langle \alpha_{\mathbf{p}} | \psi_{\mathbf{k}}^\dagger \rangle\rangle$ spinors appear.

Under the full Hamiltonian $H = H_0 + H_A$, the equation of motion for the "host" GF matrix gets modified from Eq. (7) to

$$\hat{G}(\mathbf{k},\mathbf{k}') = \delta_{\mathbf{k},\mathbf{k}'} \hat{G}^{(0)}(\mathbf{k}) + \tfrac{1}{\sqrt{N}} \textstyle\sum_{\mathbf{p}} e^{-i\mathbf{k}\cdot\mathbf{p}} \hat{G}^{(0)}(\mathbf{k}) \hat{\tau}_{\mathbf{k}} h_{\mathbf{p},\mathbf{k}'}^\dagger, \tag{32}$$

and the respective equation for the "mixed" $h^\dagger$ spinor on its right-hand side reads as

$$h_{\mathbf{p},\mathbf{k}'}^\dagger (\varepsilon - \varepsilon_0) = \frac{1}{\sqrt{N}} \sigma u m_{\mathbf{k}''} e^{i\mathbf{k}''\cdot\mathbf{p}} \hat{\tau}_{\mathbf{k}''}^\dagger \hat{G}(\mathbf{k}'',\mathbf{k}'). \tag{33}$$

Then the specific solutions for all the above mentioned GF types follow from consequent iterations of Eqs. (32) and (33).

The general strategy consists in separating, after each iteration step, all the GFs on the right-hand side that were already present in the previous steps and doing the next iteration for the resting ones, in order to compose and then fully solve an equation for each GF. The most important between them are the diagonal $\hat{G}(\mathbf{k})$ and $g_{\mathbf{p}} \equiv g_{\mathbf{p},\mathbf{p}}$ that enter the total DOS

$$\rho(\varepsilon) = \frac{1}{2\pi N} \operatorname{Im} \left(\sum_{\mathbf{k}} \hat{G}_{\mathbf{k}} + \sum_{\mathbf{p}} g_{\mathbf{p}} \right), \tag{34}$$

in the generalization of Eq. (3). Thus, a full solution for $\hat{G}(\mathbf{k})$ follows from Eq. (32) (at $\mathbf{k} = \mathbf{k}'$), after separating the same $\hat{G}(\mathbf{k})$ on the right-hand side of Eq. (33) for $h_{\mathbf{p},\mathbf{k}}^\dagger$ and applying again Eq. (32) to all $\hat{G}(\mathbf{k}',\mathbf{k})$ with $\mathbf{k}' \neq \mathbf{k}$ there. At this next iteration, a similar separation of $h_{\mathbf{p},\mathbf{k}}^\dagger$ is also done, giving rise to a respective full solution for $h_{\mathbf{p},\mathbf{k}}^\dagger$, and so on. The result, formally analogous to Eq. (8),

$$\hat{G}(\mathbf{k}) = \{[\hat{G}^{(0)}(\mathbf{k})]^{-1} - \hat{\Sigma}_{\mathbf{k}}\}^{-1}, \tag{35}$$

includes the self-energy matrix in the GE form, similar to Eq. (9): $\hat{\Sigma}_{\mathbf{k}} = c\hat{T}_{\mathbf{k}}(1 + cB_{\mathbf{k}} + \cdots)$. But here the T-matrix term,

$$c\hat{T}_{\mathbf{k}} = \frac{\eta^2 \xi^2}{1 + 2\eta^2} \frac{1}{N} \sum_{\mathbf{p}} \frac{1 + \hat{\sigma}_+ e^{2i\varphi} + \hat{\sigma}_- e^{-2i\varphi}}{\varepsilon - \varepsilon_{\text{imp}} - i\Gamma_{\text{imp}} - \Sigma_{\mathbf{p}}}, \tag{36}$$

has an important difference from the Lifshitz model form, Eq. (9), in its momentum dependence, both on the radial variable $\xi \equiv \xi_{\mathbf{k}}$ and on the angular argument $\varphi \equiv \varphi_{\mathbf{k}-\mathbf{K}}$. It also includes the single impurity level $\varepsilon_{\text{imp}} = \varepsilon_0/(1 + 2\eta^2)$ (reduced by its coupling to the host) with its imaginary part $\Gamma_{\text{imp}} = \operatorname{Im} \sum_{\mathbf{k}} \hat{\tau}_{\mathbf{k}}^\dagger \hat{G}_{\mathbf{k}} \hat{\tau}_{\mathbf{k}}$ and the "impurity" scalar self-energy:

$$\Sigma_{\mathbf{p}} = \sum_{\mathbf{p}' \neq \mathbf{p}} A_{\mathbf{p}-\mathbf{p}'} \left[F_{\mathbf{p}'-\mathbf{p}} \sum_{\mathbf{p}'' \neq \mathbf{p},\mathbf{p}'} A_{\mathbf{p}'-\mathbf{p}''} (F_{\mathbf{p}''-\mathbf{p}} + \cdots) \right]. \tag{37}$$

Here the scalar functions

$$F_{\mathbf{p}-\mathbf{p}'} = \frac{1}{N} \sum_{\mathbf{k}} e^{i\mathbf{k}\cdot(\mathbf{p}-\mathbf{p}')} \hat{\tau}_{\mathbf{k}}^\dagger \hat{G}_{\mathbf{k}} \hat{\tau}_{\mathbf{k}},$$

$$\mathrm{A}_{\mathbf{p}-\mathbf{p}'} = \frac{F_{\mathbf{p}-\mathbf{p}'}}{\varepsilon - \varepsilon_{\text{imp}} - i\Gamma_{\text{imp}} - \Sigma_{\mathbf{p}'}}$$

describe the effects of indirect interactions between impurity centers. The latter $A_{\mathbf{p}-\mathbf{p}'}$ functions also define the GE terms of the "host" self-energy $\hat{\Sigma}_{\mathbf{k}}$, along the same formal structure as in Eq. (10), while the GE structure for the scalar $\Sigma_{\mathbf{p}}$ in Eq. (37) is notably different. In this way, the solution for the diagonal "impurity" GF follows as

$$g_{\mathbf{p}} = \frac{1}{(1 + 2\eta^2)(\varepsilon - \varepsilon_{\text{imp}} - i\Gamma_{\text{imp}} - \Sigma_{\mathbf{p}})}, \tag{38}$$

and can be then used in Eq. (34). A specific feature of $\Sigma_{\mathbf{p}}$ is the random statistical distribution of its values due to random $\mathbf{p}'$ positions around given $\mathbf{p}$, with the standard deviation $\sigma = \sqrt{\overline{\Sigma_{\mathbf{p}}^2} - \overline{\Sigma_{\mathbf{p}}}^2}$. Since there is a finite range of interimpurity interactions, this deviation does not vanish in the thermodynamical limit $N \to \infty$, unlike that for $\hat{\Sigma}_{\mathbf{k}}$ (known as the self-averaging property [28]). As to the mean self-energy $\overline{\Sigma_{\mathbf{p}}}$, it can be simply included in the definition of impurity level ε_{imp}, so understood in what follows.

In this model, we present the basic secular determinant as $\det(\hat{G}_{\mathbf{k}})^{-1} = \det(\hat{G}_{\mathbf{k}}^{(0)})^{-1} + \Sigma_{\mathbf{k}}$, with the scalar self-energy

$$\Sigma_{\mathbf{k}} = \frac{\eta^2 \xi^2 (\varepsilon + \xi \cos\varphi)}{1 + 2\eta^2} \frac{1}{N} \sum_{\mathbf{p}} \frac{1}{\varepsilon - \varepsilon_{\text{imp}} - i\Gamma_{\text{imp}} - \Sigma_{\mathbf{p}}}. \tag{39}$$

Then the general Eq. (11) (written at the T-matrix level in neglect of Γ_{imp} and $\Sigma_{\mathbf{p}}$) reads

$$\varepsilon^2 = \varepsilon_0^2(\xi) + 2\tilde{c}\xi^2 \frac{\varepsilon + \xi\cos\varphi}{\varepsilon - \varepsilon_{\text{imp}}}, \tag{40}$$

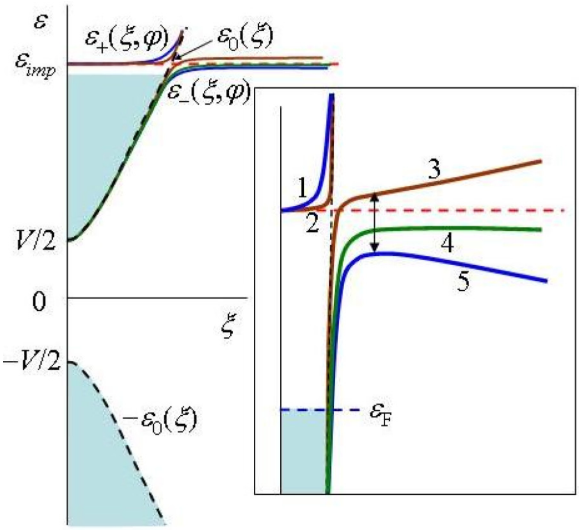

FIG. 4. Silicene dispersion laws near their splitting by the impurity level $\varepsilon_{\mathrm{imp}}$ (red dashed line) show an in-plane anisotropy. Inset resolves them for particular directions: (1) for $\varepsilon_+(\xi,\pi)$, (2) for $\varepsilon_+(\xi,0)$, (3) for $\varepsilon_-(\xi,0)$, (4) for $-(\xi,\pi/2)$, (5) for $\varepsilon_-(\xi,\pi)$. The impurity parameters are chosen as $\varepsilon_{\mathrm{imp}} = 0.1\Lambda$, $\tilde{c} = 0.005$, and the bias $V = 0.4\varepsilon_{\mathrm{imp}}$. The arrows indicate the splitting range near the impurity level $\varepsilon_{\mathrm{imp}}$.

where the reduced impurity concentration $\tilde{c} = c\eta^2/(1+2\eta^2)$ measures the quasiparticle weight transfer from impurity to band states. Equation (40) defines the dispersion laws for "host" quasiparticles that are quite close to the nonperturbed $\varepsilon_0(\xi)$ except for the $\varepsilon_{\mathrm{imp}}$ vicinity of $\sim\tilde{c}\varepsilon_{\mathrm{imp}}$ width where the splitting of two subbands is mainly developed. Within that splitting range, both subbands strongly deviate from $\varepsilon_0(\xi)$ and display a sensible in-plane anisotropy: $\varepsilon_\pm(\xi,\varphi)$ (Fig. 4), unlike the isotropically split subbands in Fig. 2. Physically, this anisotropy reflects the breakdown of local inversion symmetry for an impurity interstice at applied field bias.

Another difference from the Lifshitz model is in the possibility that, at varying bias V, the impurity level $\varepsilon_{\mathrm{imp}}$ can be crossed by the band edge $V/2$. Lastly, the presence of the ξ^2 factor in the T matrix, Eq. (36), leads to vanishing damping for long-wave quasiparticles, so that the mobility edges should correspond to shorter wavelengths (to be defined below). This implies that Bloch-like states with such short wavelengths would not make sense at energies close enough to the impurity level.

As a result, the composition of electronic spectrum in the Anderson model is more complicated than in the Lifshitz model. Here we have generally up to three subbands of the states by electrons on host sites: the two split $\varepsilon_\pm(\xi,\varphi)$ subbands and the almost nonperturbed $-\varepsilon_0(\xi)$ (valence) subband, together with a subband of the states on impurity interstices [Eq. (38)]. The important separation between bandlike and localized states can be established from the following principle. A given energy ε pertains to the range of bandlike states by virtue of those solutions of Eq. (39) that satisfy the IRM criterion, and if no such solutions exist, this energy pertains to the range of localized states by virtue of the related solutions of Eq. (38). All these states contribute to the total DOS with their particular weights defined by the residues of corresponding poles of diagonal GFs in Eq. (34).

Following this principle, one can apply the IRM criterion, Eq. (12), for almost isotropic bandlike states beyond the splitting range, $|\varepsilon - \varepsilon_{\mathrm{imp}}| \gg \tilde{c}\varepsilon_{\mathrm{imp}}$, but will need its more complete form,

$$\mathbf{k}\cdot\nabla_{\mathbf{k}}\varepsilon_\pm(\xi,\varphi) \gg \Gamma_\pm(\xi,\varphi), \tag{41}$$

within this range. Expecting the most important mobility threshold to be located below $\varepsilon_{\mathrm{imp}}$, we focus on the relevant damping term $\Gamma_-(\xi,\varphi) = \mathrm{Im}\,\Sigma_{\mathbf{k}}|\varepsilon - \varepsilon_{\mathrm{imp}}|/|\varepsilon^2 - V^2/4|$. There are several additive contributions to this term, due to Γ_{imp} and $\Sigma_{\mathbf{p}}$ in the denominator of $\hat{T}_{\mathbf{k}}$, Eq. (36), and to the GE terms such as $B_{\mathbf{k}}$. A more detailed analysis shows that the dominating contribution comes from $\Sigma_{\mathbf{p}}$, expressing the decay rates of band quasiparticles into the randomly distributed localized levels $\varepsilon_{\mathrm{imp}} + \Sigma_{\mathbf{p}}$. This contribution is already self-averaging and its average involves the probability distribution function $P(\Sigma_{\mathbf{p}})$. Since $\Sigma_{\mathbf{p}}$ by Eq. (37) is a sum of a great number of independent random values like $A_{\mathbf{p}-\mathbf{p}'}F_{\mathbf{p}'-\mathbf{p}}$, this probability distribution should take a normal form,

$$P(\Sigma_{\mathbf{p}}) = \frac{1}{\sqrt{2\pi}\sigma}\exp\left[-\frac{(\Sigma_{\mathbf{p}} - \overline{\Sigma_{\mathbf{p}}})^2}{2\sigma^2}\right],$$

that readily implies

$$\begin{aligned}\mathrm{Im}\,\Sigma_{\mathbf{k}} &= 2\tilde{c}\xi^2(\varepsilon + \xi\cos\varphi)\mathrm{Im}\,\overline{(\varepsilon - \varepsilon_{\mathrm{imp}} - \Sigma_{\mathbf{p}} + \overline{\Sigma_{\mathbf{p}}})^{-1}}\\ &= \sqrt{2\pi}\tilde{c}\xi^2\frac{\varepsilon + \xi\cos\varphi}{\sigma}\exp\left[-\frac{(\varepsilon - \varepsilon_{\mathrm{imp}})^2}{2\sigma^2}\right].\end{aligned} \tag{42}$$

Now, to evaluate the standard deviation σ, we restrict $\Sigma_{\mathbf{p}}$, Eq. (37), to its first term and approximate the interaction function by using the nonperturbed GF (see details in the Appendix):

$$\begin{aligned}F_{\mathbf{n}} &\approx \frac{1}{N}\sum_{\mathbf{k}} e^{i\mathbf{k}\cdot\mathbf{n}}\hat{\tau}_{\mathbf{k}}^\dagger\hat{G}_{\mathbf{k}}^{(0)}\hat{\tau}_{\mathbf{k}}\\ &\approx \frac{2c_0}{\pi}\left[\varepsilon K_0\left(\frac{|\mathbf{n}|}{r_\varepsilon}\right) - \Lambda\frac{|\mathbf{n}|\cos\theta}{r_\varepsilon}K_1\left(\frac{|\mathbf{n}|}{r_\varepsilon}\right)\right].\end{aligned} \tag{43}$$

Since within the relevant energy range for this case, $V/2 < \varepsilon$, the argument of McDonald functions turns to be imaginary, they can be expressed through the first and second kinds of Bessel functions [24]: $K_0(ix) = \frac{\pi}{2}[Y_0(x) + iJ_0(x)]$ and $K_1(ix) = \frac{\pi}{2}[-J_1(x) + iY_1(x)]$. Notice the presence of p-wave anisotropy by $\cos\theta = n_x/|\mathbf{n}|$ in Eq. (43), similar to that of the dispersion law, Eq. (39). Next we obtain (see Appendix)

$$\sigma^2 \approx c\sum_{\mathbf{n}\neq 0}(A_{\mathbf{n}}F_{-\mathbf{n}})^2 \sim \frac{(c_0\varepsilon_{\mathrm{imp}})^4}{(\varepsilon - \varepsilon_{\mathrm{imp}})^2}\frac{c}{c_{cr}}\ln\frac{1}{c_{cr}}, \tag{44}$$

presenting an energy-dependent $\sigma(\varepsilon)$ that grows at approach to the single impurity level $\varepsilon_{\mathrm{imp}}$, as can be expected for such resonance interactions. In Eqs. (43) and (44), $c_0 = |\varepsilon_{\mathrm{imp}}^2 - V^2/4|/\Lambda^2$ generalizes the definition in Eq. (15) for the locations of band edge $V/2$ either above and below $\varepsilon_{\mathrm{imp}}$, and the meaning of $c_{cr} = \varepsilon_{\mathrm{imp}}^2/\Lambda^2$ is explained in what follows. Using the result by Eq. (44) in Eq. (42), we conclude that the relevant damping term $\Gamma_-(\xi,\varphi)$ very steeply shoots up from exponentially low to values as high as $\sim(\tilde{c}/c_0)(\varepsilon + \xi\cos\varphi) \sim \varepsilon_{\text{imp}}$ when reaching the condition $|\varepsilon - \varepsilon_{\text{imp}}| \sim \sigma(\varepsilon)$ or

$$|\varepsilon - \varepsilon_{\text{imp}}| \sim \left(\frac{c}{c_{cr}} \ln\frac{1}{c_{cr}}\right)^{1/4} c_0 \varepsilon_{\text{imp}}. \tag{45}$$

So Eq. (45) gives just an estimate for the distance from ε_{imp} to the mobility edge ε_c. We notice that, for c close to c_{cr} and c_0, this distance exceeds the width $\tilde{c}\varepsilon_{\text{imp}}$ of the splitting range that justifies the above usage of the nonperturbed spectrum in Eq. (43). Also, the estimate by Eq. (45) defines the above mentioned minimum admitted wavelength of band quasiparticles with energies near ε_{imp}: $\lambda_{\min} \sim a/\sqrt{c_0}$.

The principal practical issue of tuned metal-insulator transition is resolved by comparing the mobility edge ε_c and the Fermi level ε_{F} whose initial position at zero bias is below ε_{imp} if the impurity concentration is smaller than the above defined critical value: $c < c_{cr}$.

Expecting the crossing of ε_{F} with ε_c at growing bias to occur outside the splitting range, we can safely estimate ε_{F} with the use of the nonperturbed DOS, Eq. (5), in Eq. (25) to result in

$$\varepsilon_{\text{F}}(V) \approx \sqrt{c\Lambda^2 + V^2/4}, \tag{46}$$

instead of Eq. (26). Then the MIT bias V_M, when the Fermi level crosses the mobility edge, is found for the Anderson model as

$$V_M \approx 2\varepsilon_{\text{imp}} \sqrt{1 - \frac{c}{c_{cr}}\left(1 + 2c^{1/4} c_{cr}^{3/4} \ln^{1/4}\frac{1}{c_{cr}}\right)}, \tag{47}$$

which is slightly below the critical value $V_{cr} = 2\varepsilon_{\text{imp}}\sqrt{1 - c/c_{cr}}$, when the Fermi level reaches ε_{imp} (as shown in Fig. 5). With further growing bias, $V > V_{cr}$, the Fermi level stays fixed near ε_{imp} while the Anderson transition for the $\varepsilon_-(\xi,\varphi)$ subband takes place when the mobility edge is attained by the band edge $V/2$. This corresponds to $V_A \approx 2\varepsilon_{\text{imp}}$.

Finally, at $V > V_A$, the impurity level ε_{imp} stays below the bottom of the almost unperturbed main band [as in Fig. 5(d)]; then $\Sigma_{\mathbf{p}}$ and so the broadening of ε_{imp} becomes exponentially small $\sim c_0 \Lambda e^{-c_0/c}$ (at $c_0 \gg c$) by virtue of similar decay of $F_{\mathbf{n}}$ in Eq. (43) and there are almost unperturbed subbands $\pm\varepsilon_0(\xi)$ in the spectrum (alike the above case of the Lifshitz model).

V. DISCUSSION AND CONCLUSIONS

The above presented considerations of electronic spectrum in biased and doped silicene within the frameworks of two models for impurity perturbation show a variety of restructuring processes in this spectrum with different dynamics for its particular subbands, derived from both the initial host subbands and from the impurity levels. The main difference between the two models is in the location of impurity energy level. In the Lifshitz model, it is ε_{loc}, Eq. (15), which closely follows the biased edge of one of the main subbands while in the Anderson model it is the bias-independent ε_{imp}, Eq. (33), that can be crossed by the biased main band edge. This determines the difference in spectrum transformations with growing bias V.

In the Lifshitz model, the initial metallic state at $V \ll V_M$ corresponds to the Fermi level ε_{F} well above ε_{loc} and the tuned MIT is realized through its dropping down to the mobility edge that emerges near ε_{loc} after the impurity subband gets decoupled from its neighbor main subband at $V > V_{\text{dec}}$. This process develops rather slowly with growing bias and requires the stronger critical level V_M the higher impurity concentration c is present in the sample. In contrast, the Anderson model provides a possibility for initial ε_{F} to be positioned below ε_{imp} and to reach the mobility edge with growing bias, the sooner the higher c is chosen. These scenarios can be suitably presented in the form of phase diagrams in terms of the relevant variables "impurity concentration–electric bias" (Fig. 6).

These diagrams for the two models clearly display the above mentioned difference in electronic phase dynamics. In the Lifshitz model, the critical value as a function of impurity concentration, $V_M(c)$, grows (logarithmically slowly) [Fig. 6(a)], while in the Anderson model this function is rapidly decreasing from its initial value $V_M(0) = 2\varepsilon_{\text{imp}}$ [Fig. 6(b)]. Also, there is a notable difference in behavior of another phase boundary in this case which defines the Anderson transition in the collapsing impurity band. In the Lifshitz model, $V_A(c)$

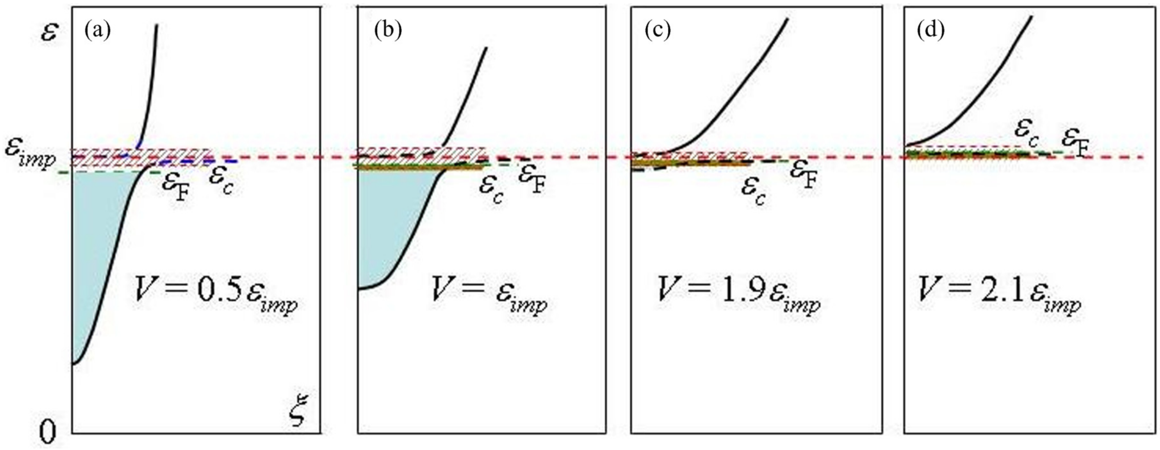

FIG. 5. Dispersion curves for silicene with Anderson impurities at the choice of their parameters as in Fig. 4. At growing bias V, the bottom of the conduction band moves towards the impurity level ε_{imp}. MIT occurs at $V_M \approx 0.84\varepsilon_{\text{imp}}$ [in between panels (a) and (b)] and the Anderson transition at $V_A \approx 2\varepsilon_{\text{imp}}$ [in between panels (c) and (d)].

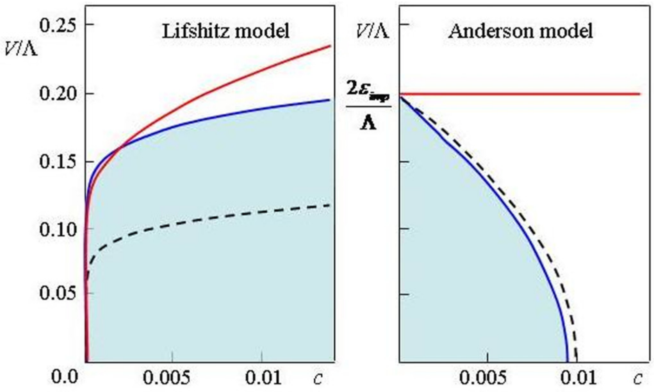

FIG. 6. Phase diagrams of electronic states in biased doped silicene in the variables “impurity concentration–electric bias” for two models of impurity perturbation. The blue areas correspond to metallic phases, separated by the Mott MIT lines V_M (dark blue) from insulating phases (white areas); Anderson transitions (collapse of impurity band) are shown by the red lines; dashed lines indicate decoupling of the impurity band from the main band, $V_{\rm dec}$ (in the Lifshitz model), or complete filling of all the states up to the impurity level $\varepsilon_{\rm imp}$ (in the Anderson model).

grows in a similar way to $V_M(c)$ and, depending on the perturbation parameter U, a crossing of these two can take place. By contrast, $V_A(c)$ in the Anderson model is practically constant: $V_A(0) \approx 2\varepsilon_{\rm imp}$.

It is readily seen from Eq. (47) that a considerable reduction of the MIT bias can be reached by driving the impurity concentration c close enough to c_{cr}. This is an essential advantage of the Anderson model scenario compared to that of the Lifshitz model, also taking into account that growing c simultaneously improves the thermal stability of tuned MIT. The other practical advantage here is in a much higher steepness $s_M = d(\varepsilon_c - \varepsilon_{\rm F})/dV$ of this transition. This is seen from the comparison of corresponding values: $V_M \approx 0.34\Lambda$, $s_M \approx 0.24$ for the Lifshitz model in Fig. 3 and $V_M \approx 0.08\Lambda$, $s_M \approx 0.42$ for the Anderson model in Fig. 5. The latter advantage is even more enforced by the fact that the damping of Fermi quasiparticles (defining the Drude resistivity of metal) at $V \to V_M$ varies slowly in the Lifshitz model, as in Eq. (24), but grows exponentially in the Anderson model, as in Eq. (42), enabling here an extremely strong variation of the doped system resistivity near the tuned MIT.

A final note is yet in order about possible consequences of the spin-orbit coupling if superimposed on the initial Hamiltonian, Eq. (1). Its known effect in silicene consists of the opening of a relatively small spectrum gap (in absence of external electric field) estimated as a few meV [20]. Over the bias range relevant for the present problem, this effect should only slightly perturb the states near the edge of the bias-induced band gap of about a tenth of an eV, with no sensible influence on the above discussed electronic phase transitions. However, theoretical possibilities for nonperturbative spin-orbit interference in these processes can be indicated for the cases of ultralow concentrations of Lifshitz impurities [Fig. 6(a)] or of Anderson impurities with concentrations close to c_{cr} [Fig. 6(b)].

Summarizing, the doped and biased silicene presents a suitable opportunity for realization of practical electronic devices with tunable electric resistivity over a very broad scale, from normal metallic to fully insulating (possibly accompanied by respective optical, thermal, etc., effects), under relatively weak bias. This regime can be optimized by a proper choice of impurity atoms, their location within the crystalline structure, and their concentration. The comparative analysis of two common models for impurity perturbation on the host electronic spectrum indicates the Anderson hybrid model (adequate for transition or rare-earth impurities in silicene) to be more promising for such purpose. Comparing the present system to the other known material with tunable gap, bigraphene, where similar doping effects were recently considered [29], an advantage of the silicene host is seen in the simpler structure of its electronic spectrum. Experimental checks on the proposed regimes of doping and tunable phase transitions could better determine the field for future studies and probably open some new possibilities in this direction.

ACKNOWLEDGMENTS

Y.G.P. is grateful for the support from the Portuguese FCT through Project No. PTDC/FIS/120055/2010. The work of V.M.L. was partly supported by the Special Program for Fundamental Research of the Division of Physics and Astronomy of the National Academy of Sciences of Ukraine.

APPENDIX

Quasimomentum sums over the Brillouin zone (BZ) commonly result in certain analytic functions of other relevant arguments (such as position vectors, energy, etc.), and their calculation is done by passing from sum to integral,

$$\frac{1}{N}\sum_{\mathbf{k}} f_{\mathbf{k}} = \frac{1}{v_{BZ}}\int_{BZ} f_{\mathbf{k}} d\mathbf{k}, \qquad \text{(A1)}$$

where v_{BZ} is the BZ volume. In the present case, the 2D BZ consists of two equilateral triangles with side $\sqrt{3}K$, each centered in a nodal point, and the above integration of a function $f_{\mathbf{k}}$ that decays fast enough away from the nodal points can be approximately done in the radial and angular variables ξ, φ over the circle of radius Λ:

$$\frac{1}{v_{BZ}}\int_{BZ} f_{\mathbf{k}} d\mathbf{k} \approx \frac{1}{\pi\Lambda^2}\int_0^{\Lambda}\xi d\xi\int_0^{2\pi} d\varphi f(\xi,\varphi). \qquad \text{(A2)}$$

Among all the functions that have no such decay and so do not admit such approximation, we distinguish the important case of plane wave, $f_{\mathbf{k}} = e^{i\mathbf{k}\cdot\mathbf{n}}$, providing an exact result:

$$\frac{1}{N}\sum_{\mathbf{k}} e^{i\mathbf{k}\cdot\mathbf{n}} = \delta(\mathbf{n}), \qquad \text{(A3)}$$

where the discrete Dirac delta is $\delta(\mathbf{n}) = 0$ for any $\mathbf{n}$ joining two lattice sites (or two interstices) and $\delta(0) = 1$.

Now we apply these techniques to the calculation of the basic interaction functions $A_{\mathbf{n}}$ and $F_{\mathbf{n}}$ in the approximation of a nonperturbed spectrum. Starting from the definition in the

Lifshitz model, Eq. (10), we obtain (at $\varepsilon^2 < V^2/4$)

$$\begin{aligned} A_{j,\mathbf{n}} &\approx \frac{T_j(\varepsilon \pm V/2)}{N}\sum_{\mathbf{k}} \frac{e^{i\mathbf{k}\cdot\mathbf{n}}}{\varepsilon^2 - V^2/4-\xi^2} \\ &\approx \frac{T_j(2\varepsilon\pm V)}{\Lambda^2}\int_0^\infty \xi d\xi \frac{J_0(\xi|\mathbf{n}|/\hbar v_{\mathrm{F}})}{\varepsilon^2 - V^2/4-\xi^2}, \\ &= \frac{T_j(\varepsilon\pm V/2)}{\Lambda^2}K_0(|\mathbf{n}|/r_\varepsilon), \end{aligned}$$

the result in Eq. (14). In particular, its asymptotics at $n \gg r_\varepsilon$ defines the broadening of the localized impurity level at $c \ll c_0$, by the criterion $c\,\mathrm{Im}\,B_1 \sim 1$, where

$$\begin{aligned} \mathrm{Im}\,B_1 &= \mathrm{Im}\sum_{\mathbf{n}\neq 0}\frac{1}{1-A_{1,\mathbf{n}}^2} \approx \frac{\pi}{a^2}\int_a^\infty \delta\big(1-A_{1,\mathbf{r}}^2\big)rdr \\ &\approx \frac{\pi r_\varepsilon^2}{a^2}\ln\frac{c_0\Lambda^2}{V(\varepsilon-\varepsilon_{\mathrm{loc}})} \approx \frac{\pi}{c_0}\ln\frac{c_0\Lambda^2}{V(\varepsilon-\varepsilon_{\mathrm{loc}})}. \end{aligned}$$

Therefore the above criterion takes place at $|\varepsilon-\varepsilon_{\mathrm{loc}}| \sim (c_0\Lambda^2/V)e^{-c_0/c}$, as indicated after Eq. (30).

For the Anderson model, with the definition by Eq. (37), we have (at $\varepsilon^2 > V^2/4$)

$$\begin{aligned} F_{\mathbf{n}} &\approx \frac{2}{N}\sum_{\mathbf{k}} e^{i\mathbf{k}\cdot\mathbf{n}}\xi^2\frac{\varepsilon+\xi\cos\varphi}{\varepsilon^2-V^2/4-\xi^2} \\ &= -\frac{2}{N}\sum_{\mathbf{k}} e^{i\mathbf{k}\cdot\mathbf{n}}(\varepsilon+\xi\cos\varphi) \\ &\quad + \frac{2(\varepsilon^2-V^2/4)}{N}\sum_{\mathbf{k}}\frac{e^{i\mathbf{k}\cdot\mathbf{n}}(\varepsilon+\xi\cos\varphi)}{\varepsilon^2-V^2/4-\xi^2}. \end{aligned} \tag{A4}$$

Then, applying Eq. (A3) to the first sum on the right-hand side of Eq. (A4) gives two terms proportional to $\delta(\mathbf{n})$ and $d\delta(\mathbf{n})/dn_x$, which vanish for any $\mathbf{n}\neq 0$. The second sum is treated by means of Eq. (A2) as follows:

$$\begin{aligned} &\frac{2}{N}\sum_{\mathbf{k}} e^{i\mathbf{k}\cdot\mathbf{n}}\frac{\varepsilon+\xi\cos\varphi}{\varepsilon^2-V^2/4-\xi^2} \\ &\approx \frac{2}{\pi\Lambda^2}\int_0^\Lambda \frac{\xi d\xi}{\varepsilon^2-V^2/4-\xi^2} \\ &\times\left[\varepsilon J_0\left(\frac{\xi|\mathbf{n}|}{\hbar v_{\mathrm{F}}}\right)+\xi J_1\left(\frac{\xi|\mathbf{n}|}{\hbar v_{\mathrm{F}}}\right)\cos\theta\right], \end{aligned}$$

and, after extending the upper integration limit to infinity, the exact formulas can be used:

$$\begin{aligned} \int_0^\infty \frac{xJ_0(x)dx}{b^2-x^2} &= \frac{i\pi}{2}H_0^{(2)}(b), \\ \int_0^\infty \frac{x^2J_1(x)dx}{b^2-x^2} &= \frac{i\pi}{2}bH_1^{(2)}(b), \end{aligned} \tag{A5}$$

with the second kind of Hankel functions $H_l^{(2)}(x)$ [24] and $b = |\mathbf{n}|/|r_\varepsilon|$. This leads finally to the result of Eq. (43).

Now let us consider the standard deviation of the random scalar self-energy $\Sigma_{\mathbf{p}}$:

$$\sigma^2 = \overline{\Sigma_{\mathbf{p}}^2} - \overline{\Sigma_{\mathbf{p}}}^2, \tag{A6}$$

restricting the definition of $\Sigma_{\mathbf{p}}$ in Eq. (37) to its first term, of the lowest linear order in impurity concentration. Then we present

$$\begin{aligned} \Sigma_{\mathbf{p}} &\approx (\varepsilon-\varepsilon_{\mathrm{imp}})^{-1}\sum_{\mathbf{n}\neq 0} c_{\mathbf{n}}F_{\mathbf{n}}F_{-\mathbf{n}}, \\ \Sigma_{\mathbf{p}}^2 &\approx (\varepsilon-\varepsilon_{\mathrm{imp}})^{-2}\sum_{\mathbf{n},\mathbf{n}'\neq 0} c_{\mathbf{n}}c_{\mathbf{n}'}F_{\mathbf{n}}F_{-\mathbf{n}}F_{\mathbf{n}'}F_{-\mathbf{n}'}, \end{aligned} \tag{A7}$$

where the random numbers $c_{\mathbf{n}}$ of impurity occupation at $\mathbf{n}$th interstice take the values 1 with probability c and 0 with probability $1-c$ and the nonrenormalized denominators $\varepsilon-\varepsilon_{\mathrm{imp}}$ correspond to the adopted precision to the lowest order in c. Using this in Eq. (A6) and taking into account that $\overline{c_{\mathbf{n}}} = c$, $\overline{c_{\mathbf{n}}c_{\mathbf{n}'}} = c^2$ at $\mathbf{n}\neq\mathbf{n}'$ and $\overline{c_{\mathbf{n}}^2} = c$, we obtain

$$\sigma^2 = c(1-c)(\varepsilon-\varepsilon_{\mathrm{imp}})^{-2}\sum_{\mathbf{n}\neq 0}(F_{\mathbf{n}}F_{-\mathbf{n}})^2. \tag{A8}$$

The decisive point in the evaluation of this sum over interstices is that the products $F_{\mathbf{n}}F_{-\mathbf{n}}$ do not include Fourier components with coinciding quasimomenta [see after Eq. (10)]. Using the inverse orthogonality relation to Eq. (A3), $N^{-1}\sum_{\mathbf{n}} e^{i\mathbf{k}\cdot\mathbf{n}} = \delta(\mathbf{k})$, we present the relevant sum as

$$\sum_{\mathbf{n}\neq 0}(F_{\mathbf{n}}F_{-\mathbf{n}})^2 = -F_0^4 + S,$$

where $F_0^4 \approx (c_0\varepsilon)^4$ is prevailed by

$$S = \frac{1}{N^3}\sum_{\mathbf{k}_1,\mathbf{k}_2,\mathbf{k}_3} f_{\mathbf{k}_1}f_{\mathbf{k}_2}f_{\mathbf{k}_3}f_{\mathbf{k}_1+\mathbf{k}_2-\mathbf{k}_3},$$

with

$$f_{\mathbf{k}} = 2(\varepsilon^2-V^2/4)\frac{\varepsilon+\xi\cos\varphi}{\varepsilon^2-V^2/4-\xi^2}.$$

This triple sum in $\mathbf{k}_j$ is dominated by its real part, mainly due to the short-wave contributions from $\xi \gg \sqrt{\varepsilon^2-V^2/4} \approx \sqrt{c_0}\Lambda$, and it can be estimated by the triple integral in $\xi_j = \hbar v_{\mathrm{F}}k_j$:

$$\begin{aligned} S &\sim (2c_0\varepsilon_{\mathrm{imp}})^4\Lambda^2\int_{\varepsilon_{\mathrm{imp}}}^\Lambda\frac{d\xi_1}{\xi_1}\int_{\varepsilon_{\mathrm{imp}}}^\Lambda\frac{d\xi_2}{\xi_2}\int_{\varepsilon_{\mathrm{imp}}}^\Lambda\frac{d\xi_3}{\xi_3\big(\xi_1^2+\xi_2^2+\xi_3^2\big)} \\ &\sim \frac{(c_0\varepsilon_{\mathrm{imp}})^4}{c_{cr}}\ln\frac{1}{c_{cr}} \end{aligned} \tag{A9}$$

(the φ-oscillating terms in $f_{\mathbf{k}}$ are not important for this result). This readily leads to the expressions in Eqs. (44) and (45).

Finally, the broadening of the localized impurity level at $V/2 > \varepsilon_{\mathrm{imp}}$ is obtained in the same way as shown above for the case of the Lifshitz model at $c \ll c_0$, with the only difference for the pre-exponential factor $c_0\Lambda$ here resulting from the dominant contribution by the second term in Eq. (43).

[1] K. S. Novoselov, A. K. Geim, S. V. Morozov, D. Jiang, M. I Katsnelson, I. V. Grigorieva, S. V. Dubonos, and A. A. Firsov, Nature (London) **438**, 197 (2005).
[2] E. V. Castro, K. S. Novoselov, S. V. Morozov, N. M. R. Peres, J. M. B. Lopes dos Santos, J. Nilsson, F. Guinea, A. K. Geim, and A. H. Castro Neto, Phys. Rev. Lett. **99**, 216802 (2007).
[3] G. G. Guzman-Verri and L. C. Lew Yan Voon, Phys. Rev. B **76**, 075131 (2007).
[4] Z. Ni, Q. Liu, K. Tang, J. Zheng, J. Zhou, R. Qin, Z. Gao, D. Yu, and J. Lu, Nano Lett. **12**, 113 (2012).
[5] L. Stille, C. J. Tabert, and E. J. Nicol, Phys. Rev. B **86**, 195405 (2012).
[6] R. Quhe, R. Fei, Q. Liu, J. Zheng, H. Li, C. Xu, Z. Ni, Y. Wang, D. Yu, Z. Gao, and J. Lu, Sci. Rep. **2**, 853 (2012).
[7] N. D. Drummond, V. Zolyomi, and V. I. Fal'ko, Phys. Rev. B **85**, 075423 (2012).
[8] L. Tao, E. Cinquanta, D. Chiappe, C. Grazianelli, M. Fanciulli, M. Dubey, A. Molle, and D. Akinwande, Nat. Nanotechnol. **10**, 227 (2015).
[9] L. Meng, Y. Wang, L. Zhang, S. Du, R. Wu, L. Li, Y. Zhang, G. Li, H. Zhou, W. A. Hofer, and H.-J. Gao, Nano Lett. **13**, 685 (2013).
[10] H. J. W. Zandvliet, Nano Today **9**, 691 (2014).
[11] B. I. Shklovskii and A. L. Efros, *Electronic Properties of Doped Semiconductors* (Springer-Verlag, Berlin, 1984).
[12] S. M. Sze, *Physics of Semiconductor Devices* (Wiley-Interscience, New York, 1969).
[13] A. P. Roth, J. B. Webb, and D. F. Williams, Phys. Rev. B **25**, 7836 (1982).
[14] G. D. Watkins, Physica B+C **117-118**, 9 (1983).
[15] N. F. Mott, Adv. Phys. **16**, 49 (1967).
[16] I. M. Lifshitz, JETP **12**, 117 (1942).
[17] P. W. Anderson, Phys. Rev. **124**, 41 (1961).
[18] S. Cahangirov, M. Topsakal, E. Akturk, H. Sahin, and S. Ciraci, Phys. Rev. Lett. **102**, 236804 (2009).
[19] D. Jose and A. Datta, Acc. Chem. Res. **47**, 593 (2014); J. Phys. Chem. C **116**, 24639 (2012).
[20] C.-C. Liu, H. Jiang, and Y. Yao, Phys. Rev. B **84**, 195430 (2011).
[21] M. A. Ivanov, Sov. Phys. Solid State **12**, 1508 (1971).
[22] M. A. Ivanov, V. M. Loktev, and Y. G. Pogorelov, Phys. Rep. **153**, 209 (1987).
[23] A. F. Ioffe and R. A. Regel, Prog. Semicond. **4**, 237 (1960).
[24] M. Abramowitz and I. Stegun, *Handbook of Mathematical Functions: With Formulas, Graphs, and Mathematical Tables* (National Bureau of Standards, Washington, 1972), p. 374.
[25] R. Corless, G. Gonnet, D. Hare, D. Jeffrey, and D. Knuth, Adv. Comput. Math. **5**, 329 (1996).
[26] In fact, the real limits for the $\varepsilon_{\mathrm{imp}}$ band from the IRM criterion, Eq. (12) (the Mott mobility edges), lie somewhat deeper within this band, but as far as $c_0 \ll c$ they do not sensibly change the above estimate for Δ_{imp}.
[27] E. Schibli and A. G. Milnes, Mater. Sci. Eng. **2**, 173 (1967).
[28] I. M. Lifshitz, S. A. Gredescul, and L. A. Pastur, *Introduction to the Theory of Disordered Systems* (Wiley, New York, 1988).
[29] Y. G. Pogorelov, M. C. Santos, and V. M. Loktev, Phys. Rev. B **92**, 075401 (2015).